

Exploring the Electronic and Magnetic Properties of New Metal Halides from Bulk to Two-Dimensional Monolayer: RuX₃ (X=Br, I)

F. Ersan,^{1,2} E. Vatansever,³ S. Sarikurt,³ Y.Yüksel,³ Y. Kadioglu,^{1,2}
H. D. Ozaydin,¹ O.Üzengi Aktürk,^{4,5} U. Akıncı,^{3,*} and E. Aktürk^{1,5,†}

¹*Department of Physics, Adnan Menderes University, Aydın 09010, Turkey*

²*Department of Physics, Bilkent University, Ankara 06800, Turkey.*

³*Dokuz Eylül University, Faculty of Science, Physics Department, Tınaztepe Campus, 35390 zmir, Turkey*

⁴*Department of Electrical and Electronic Engineering, Adnan Menderes University, 09100 Aydın, Turkey*

⁵*Nanotechnology Application and Research Center, Adnan Menderes University, Aydın 09010, Turkey*

(Dated: April 6, 2018)

Theoretical and experimental studies present that metal halogens in MX₃ forms can show very interesting electronic and magnetic properties in their bulk and monolayer phases. Many MX₃ materials have layered structures in their bulk phases, while RuBr₃ and RuI₃ have one-dimensional chains in plane. In this paper, we show that these metal halogens can also form two-dimensional layered structures in the bulk phase similar to other metal halogens, and cleavage energy values confirm that the monolayers of RuX₃ can be possible to be synthesised. We also find that monolayers of RuX₃ prefer ferromagnetic spin orientation in the plane for Ru atoms. Their ferromagnetic ground state, however, changes to antiferromagnetic zigzag state after U is included. Calculations using PBE+U with SOC predict indirect band gap of 0.70 eV and 0.32 eV for the optimized structure of RuBr₃ and RuI₃, respectively. Calculation based on the Monte Carlo simulations reveal interesting magnetic properties of RuBr₃, such as large Curie temperature against RuI₃, both in bulk and monolayer cases. Moreover, as a result of varying exchange couplings between neighboring magnetic moments, magnetic properties of RuBr₃ and RuI₃ can undergo drastic changes from bulk to monolayer. We hope our findings can be useful to attempt to fabricate the bulk and monolayer of RuBr₃ and RuI₃.

I. INTRODUCTION

Recently, the family of transition metal trihalides MX₃, where M is a metal cation (M= Ti, V, Cr, Fe, Mo, Ru, Rh, Ir) and X is halogen anion (X= Cl, Br, I), have received increasing attention due to their potential applications in spintronics.¹⁻⁷ Even though these materials have been known for more than 50 years,⁸⁻¹¹ and their structure is well-investigated; only a few three-dimensional (3D) layered transition metal halides have been observed experimentally.^{12,13} In recent years, it is possible to exfoliate these 3D layered crystals down to two-dimensional (2D) monolayers, due to the weak interlayer van der Waals (vdW) interactions.^{14,15} For instance, Weber *et al.*¹⁶ report the exfoliation of the magnetic semiconductor α -RuCl₃ into the first halide monolayers and investigations of its in-plane structure show that it is retained during the exfoliation process. Huang *et al.* use magneto-optical Kerr effect (MOKE) microscopy to demonstrate the monolayer CrI₃ is an Ising model ferromagnet with out-of-plane spin orientation. They find out that its Curie temperature of 45 K is only slight lower than 61 K of the bulk crystal,¹⁷ consistent with a weak interlayer coupling.¹⁸ Similarly very recently, McGuire *et al.*¹⁹ both experimentally and theoretically focus on the crystallographic and magnetic properties of transition metal compound α -MoCl₃ behavior above the room temperature.

Transition metal trihalides provide a rich family of ma-

terials with a wide range of electronic, optical and mechanical properties in which also low dimensional magnetism can be examined, and therefore rapidly increasing theoretical researches exists on this area.²⁰⁻²⁴ In our previous study, we systematically investigate the electronic and magnetic properties of an α -RuCl₃ monolayer using DFT and MC simulations,²⁵ and our cleavage energy calculations give smaller value than that of graphite, which means that the α -RuCl₃ monolayer can be easily obtained from its bulk phase and also we find that it is stable 2D intrinsic ferromagnetic semiconductor. Similarly, a class of 2D ferromagnetic monolayers CrX₃ (X= Cl, Br, I) is studied by Liu *et al.*²⁶ by using first principle calculations combined with MC simulations based on the Ising Model. They confirm that the feasibility of exfoliation from their layered bulk phase by the small cleavage energy and all the ground states monolayers are semiconducting with band gaps of 2.28, 1.76 and 1.09 eV for CrCl₃, CrBr₃, CrI₃, respectively. Furthermore, the estimated Curie temperatures for CrCl₃, CrBr₃, CrI₃ are found 66, 86, 107 K, respectively. Different from this study, among the chromium trihalides, the CrI₃ is also studied by another group both in experimentally and theoretically²⁷ since it is the simplest to prepare due to iodine can be handled relatively easy solid at room temperature. They find that an easily cleavable, layered and insulating ferromagnet with Curie temperature of 61 K. Similarly, Huang *et al.*²⁸ examine RuX₃ (X=Cl, Br, I) monolayers and use only RuI₃ monolayer as an ex-

emplary material to study their electronic and magnetic properties by using first-principle calculations. Their result reveal that the ground state of the RuI₃ monolayer is ferromagnetic with estimated Curie temperature to above the room temperature ~ 360 K. Nevertheless, *ab-initio* molecular dynamics (AIMD) simulations confirm its thermal stability at 500 K and also a clear Dirac cone in the spin-down channel appears at the K -point in the Brillouin zone near the Fermi level of its band structure. Similarly, relying on our previous experience,²⁵ in this work we both focus on from bulk to monolayer RuI₃ and RuBr₃ electronic and magnetic properties in detail. Our results which are systematically investigated below are incompatible with the previous study. Since, our theoretical results demonstrate that RuBr₃ and RuI₃ can be stable in bulk form and monolayers of them can be obtained from their bulk phases by cleavage methods. We have obtained the possible magnetic ground state for bulk and monolayer forms of RuBr₃ and RuI₃ using PBE, PBE+SOC and U+SOC calculations. The FM spin orientation is the most favorable configuration for PBE and PBE+SOC results, while Zigzag spin orientation is favored after adding the Hubbard parameter. Hence, with considering the Hubbard U correction, the favored spin orientation can be altered to antiferromagnetic zigzag situation and these RuX₃ monolayer structures have suitable band gaps for various optoelectronic device applications. Afterwards, we have obtained the magnetic exchange coupling constants and magnetic anisotropy energies from the density functional theory calculations. Using these parameters, we have also performed Monte Carlo (MC) simulations, and estimated the Curie temperatures for RuBr₃ and RuI₃. According to our MC data, both structures in bulk and monolayer forms are found to be magnetically ordered at temperatures well below the room temperature.

II. COMPUTATIONAL METHODOLOGY

Density functional theory (DFT) calculations were performed by using VASP package^{29,30} within generalized gradient approximation (GGA).³¹ The Perdew-Burke-Ernzerhof (PBE) functionals were used for the exchange-correlation potential³² and the Projector Augmented Wave (PAW) pseudo potentials were adopted.^{33,34} A cut-off energy of 400 eV for the plane wave basis set was used. Monkhorst-Pack³⁵ mesh of $16 \times 8 \times 1$ (for bulk) and $16 \times 8 \times 1$ (for monolayer) were employed for the Brillouin zone integration. A supercell with a 24 \AA vacuum distance was used in order to avoid interactions between two adjacent monolayer system when the periodic conditions are employed. The geometrical configurations were optimized by fully relaxing the atomic structures, until Hellmann-Feynman forces acting on each atom is reduced to less than 0.002 eV/\AA . The convergence of the total energy is achieved until the energy difference between successive iteration steps are less than 10^{-5} eV . Phonon dis-

persion curves were obtained by PHONOPY code³⁶ for the $2 \times 2 \times 1$ supercell and displacement of 0.01 \AA from the equilibrium atomic positions. Finite temperature AIMD calculations within Verlet algorithm were performed for thermal stability test. We used Nosé thermostat for the duration of 2 picoseconds (ps) at 500 K for $3 \times 3 \times 1$ α -RuX₃ (X=Br, I) supercells.

To elucidate the magnetic structure of RuX₃, and the nearest, second-nearest, and third-nearest neighbor exchange-coupling parameters (J_1 , J_2 and J_3 , respectively), we adapt the total energy values obtained from DFT calculations for different magnetic configurations to the Heisenberg Spin Hamiltonian:

$$\mathcal{H} = -J_1 \sum_{\langle ij \rangle} \mathbf{S}_i \cdot \mathbf{S}_j - J_2 \sum_{\langle\langle ik \rangle\rangle} \mathbf{S}_i \cdot \mathbf{S}_k - J_3 \sum_{\langle\langle\langle il \rangle\rangle\rangle} \mathbf{S}_i \cdot \mathbf{S}_l + k_x \sum_i (S_i^x)^2 + k_y \sum_i (S_i^y)^2, \quad (1)$$

where \mathbf{S}_i is the spin at the Ru site i and (i, j) , (i, k) and (i, l) stand for the nearest, second-nearest, and third-nearest Ru atoms, respectively. And k_x and k_y denote the out-of-plane magnetic anisotropy constants, respectively. The numerical values of k_x and k_y are obtained from magneto-crystalline anisotropy energies (MAE).

By mapping the DFT energies to the Heisenberg Hamiltonian, J_1 , J_2 and J_3 can be calculated from following equations:³⁷

$$E_{FM/Neel} = E_0 - (\pm 3J_1 + 6J_2 \pm 3J_3)S^2 \quad (2)$$

and

$$E_{Zigzag/Stripy} = E_0 - (\pm J_1 - 2J_2 \mp 3J_3)S^2 \quad (3)$$

The calculated J_1 , J_2 , J_3 exchange-coupling parameters, in-plane (E[100]-E[010]) and out-of-plane (E[100]-E[001]) MAEs and magnetic anisotropy constants can be found in Supplementary Material (S.M) Table S3 and S4 for both RuBr₃ and RuI₃. The Curie temperature was calculated by using these exchange-coupling parameters in MC simulations based on the Heisenberg model.

III. FROM BULK TO TWO-DIMENSIONAL MONOLAYER RUX₃; DFT CALCULATIONS

Transition metal halides can be observed in several types of space groups such as C2/m, Pmmm, P6₃/mcm, P3₁12. Among them metal halide crystal structure in P3₁12 space group has equidistant metal atoms in the cell. Experimentally RuBr₃ can have Pmmm space group at low temperature while it has P6₃/mcm space group at high temperatures, and RuI₃ has P6₃/mcm space group at room temperature.³⁸ In this paper we study only bulk RuBr₃ and RuI₃ structure in P3₁12 space group which is valid for RuCl₃ (see Fig. 1). And also we obtain and investigate their stable monolayer forms. We initially constructed the bulk RuBr₃ and RuI₃ structures, and

we obtained the optimized lattice constants as $a=6.25$ Å, $b=10.83$ Å, $c=6.31$ Å for RuBr_3 , $a=6.77$ Å, $b=11.67$ Å and $c=6.71$ Å for RuI_3 . Since they have not been synthesized in RuCl_3 bulk type, we expose them in dynamical stability tests such as phonon and molecular dynamic (MD) calculations. Obtained phonon band structures and corresponding thermodynamic variables are given in S.M Fig.S1. As can be seen in Fig.S1 both of bulk RuX_3 structures are dynamically stable for $P3_112$ space group, and their heat capacities trend follow the Dulong-Petit limit after around 200 K. The AIMD calculations also showed that bulk form of RuX_3 structures are thermally stable at 500K for 2 ps. After optimization and stability calculations we examine their electronic properties, according to standard PBE calculations we found that both of bulk RuX_3 structures are metal. Bader charge analysis indicates that each Ru atom in the bulk RuBr_3 gives 0.70 electrons (e^-) and each Br atom takes $0.23 e^-$. These values are $0.30 e^-$ for Ru atoms and $0.10 e^-$ for I atoms in the bulk RuI_3 structure. To examine the favorable spin oriented status in the bulk RuX_3 structures four types of spin configurations are considered (FM, AFM-Neél, AFM-Zigzag and AFM-Stripy) for ruthenium atoms as seen in Fig. 2. We performed these calculations for three different DFT methods such as PBE, PBE+SOC (spin-orbit coupling) and U+SOC (for Hubbard $U=1.5$ eV) calculations. According to the calculations FM spin orientation is favorable for PBE and PBE+SOC results, while Zigzag spin orientation is favored after adding the Hubbard parameter (please see S.M Table S1 for relative energies, and band structures of bulk RuX_3). Finally, we tested the possibility of the exfoliation techniques to get few layers of monolayer from their bulk forms. For these calculations bulk RuX_3 structures are extended in z -direction and four layered RuX_3 structures are created, and then we implemented a fracture in the bulk after four periodic layers and systematically increased this fracture distance; at the end we calculated the corresponding cleavage energy (CE) (Fig. 1). RuCl_3 results are taken from our previous study.²⁵ As can be seen increasing of the halogens rows in the periodic table enhances the cleavage energy. But calculated energies are comparable with graphite, and other MX_3 materials.^{3,8,20,21,26,27,39}

Monolayer RuBr_3 and RuI_3 structures are constructed in hexagonal unitcell, which have lattice constants of $a=6.25$ Å, and $a=6.78$ Å for RuBr_3 and RuI_3 , respectively. This lattice value is 5.92 Å for RuCl_3 ²⁵ as expected lattice constants increase by increasing the atomic radii from chlorine to iodine. Pauling electronegativity values are 2.20 for Ru atom 2.96 for Br and 2.66 for I atoms, this electronegativity difference results more electron transferring from Ru atoms to Br atoms than I atoms. According to Bader charge analysis while each Ru atom in RuBr_3 loses 0.72 electrons (e^-), this value is $0.32 e^-$ in RuI_3 monolayer. This charge transfer interpretable such as there is more strength bond between Ru and Br atoms according to Ru-I atoms. Similar dynamical tests

which are performed for bulk RuX_3 structures are also performed for monolayers. Phonon band structures and their partial density of states (PDOS) of RuX_3 monolayers are illustrated in Fig. 1. Phonon dispersions are obtained by using PHONOPY code which is based on density functional perturbation theory as implemented in VASP. As can be seen, all phonon branches have positive frequency values in the whole Brillouin Zone (BZ) which implies the dynamical stability at $T\sim 0$ K. As mentioned later, spin-polarization is more effective in RuBr_3 with respect to RuI_3 monolayer. Thus, phonon band structure of RuBr_3 obtained with spin-polarized calculation due to it has large imaginary frequencies for out-of-plane acoustical branch (ZA) for spin-unpolarized status. In addition, phonon band structure of RuI_3 monolayer has a local minimum at the M high symmetry point for the ZA, which is associated with Kohn anomalies. Thermal stability tests are performed by AIMD calculations. All RuX_3 structures subjected to 500K temperature for 2 ps. At the end of calculations both of RuBr_3 and RuI_3 monolayers preserved their optimized atomic configuration which are obtained at $T=0$ K calculations. This means that RuX_3 monolayers can be stable at room temperature and at least slightly above it. This conclusion is very important to utilize them in device technology. After the stability tests we start to investigate to determine their favorable magnetic ground states. For this examination, we changed the hexagonal RuX_3 unitcell to the rectangular cell and considered four types of spin configurations similar to bulk ones as seen in Fig. 2. We performed geometric optimization calculations to the structures for all considered magnetic orientation status until the pressure on the cell is approximately zero, with and without spin-orbit coupling (SOC) effect. According to these PBE and PBE+SOC calculations we found that FM state is energetically favorable spin oriented status for both RuBr_3 and RuI_3 monolayers. But AFM-Stripy- RuBr_3 has only 86 meV higher energy than FM state and this difference is reduced to 67 meV when the SOC is added in calculations. SOC is more effective in RuI_3 monolayer, energy difference between FM and Stripy state is 119 meV without SOC effects, while it becomes 10 meV with SOC contribution. Relative energy differences for other spin orientation states can be found in S.M Table S2. Each FM- RuX_3 structure has $4\mu_B$ magnetic moment in per rectangular cell and each Ru atom in the cell has $1\mu_B$ magnetic moment. We also calculated the cohesive energies of FM- RuX_3 structures to determine the strength of cohesion between the Ru and X atoms and we estimate 13.67 eV and 12.81 eV for per RuBr_3 and RuI_3 quartet atoms, respectively. Dominant orbital contribution to the electronic structure comes from Ru d and halogen p orbitals, Fig. 3 shows the electronic PDOS of RuX_3 monolayers for various spin-orientation and with (w) and without (w/o) SOC effect. As seen in Fig. 3 a) both of monolayers have large band gap for spin up channel, ordered in 1.65 eV and 1.45 eV for FM- RuBr_3 and FM- RuI_3 ,

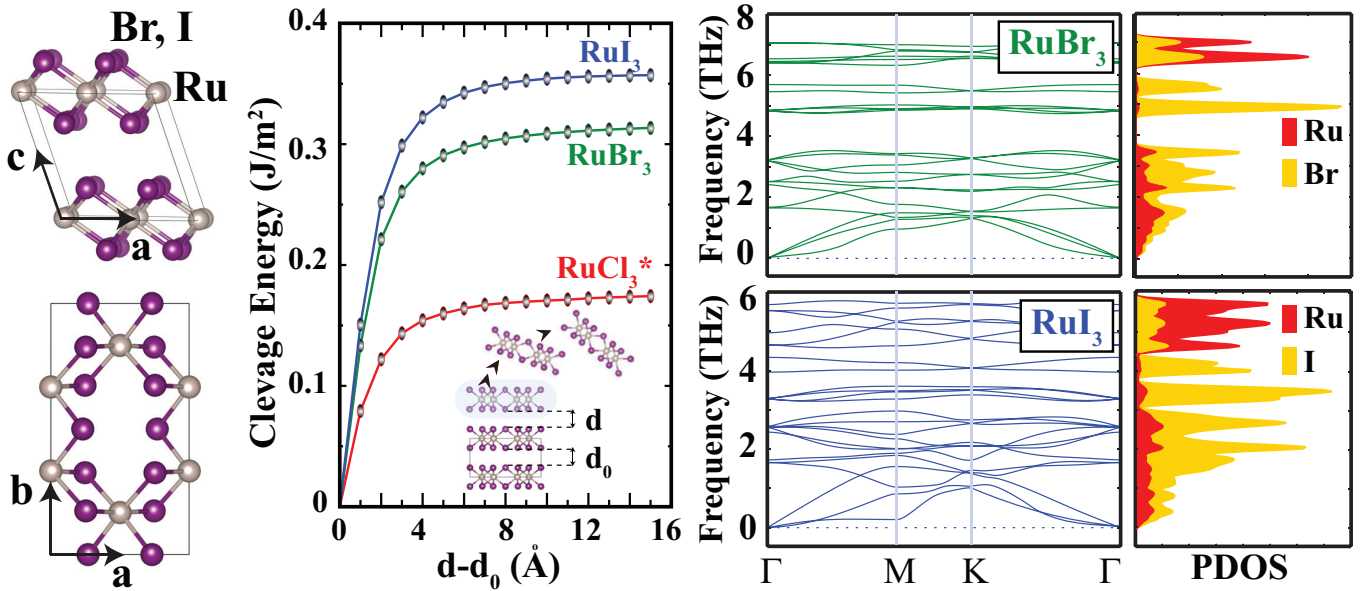


Figure 1. (Color online) Top and side view of bulk ($P312$ space group) RuX_3 structure is shown at left panel. Middle panel for cleavage energy as a function of separation between the two fractured parts. The fracture distance is denoted as d and the equilibrium interlayer distance of ruthenium trihalides as d_0 . Inside the graph: side view of bulk $a\text{-RuX}_3$ used to simulate the exfoliation procedure, RuCl_3 results taken from Sarikurt *et al.* study.²⁵ Phonon band structures and corresponding PDOS of hexagonal RuX_3 monolayer structures are illustrated at right panel.

while density of states are very close to each other for spin down channels (There is a 20 meV gap between the DOSs for FM- RuBr_3 , while this gap reaches to 100 meV for FM- RuI_3). For FM- RuBr_3 spin up state, two fold e_g (d_{z^2} and $d_{x^2 - y^2}$) orbitals and three fold t_{2g} (d_{xy} , d_{yz} and d_{xz}) orbitals contribute equally to the valence band maximum (VBM), while there are just t_{2g} orbitals contribution in conduction band minimum (CBM) and between 1.7-1.9 eV. Also dominant contribution comes from t_{2g} orbitals for spin down channel around the Fermi level, and again there are only t_{2g} orbitals between 1.8-2.0 eV in spin down. Br atom p orbitals give approximately equal contribution around VBM and CBM for both spin up and down channels (see S.M Fig.S3). For FM- RuI_3 spin up two fold e_g orbitals are dominant at VBM and at CBM, t_{2g} orbitals contributions start ~ 0.2 eV lower energy from VBM, while there are not in CB. Spin down states possess similar situation with FM- RuBr_3 spin down channel. In plane p orbitals (p_x , p_y) of iodine give major contribution to the VBM for spin up state as seen in Fig.S3. By including SOC effect in calculation for FM- RuBr_3 system gains metallic character, while FM- RuI_3 preserves semiconducting behavior (Fig. 3b). Electric and magnetic properties of such layered metal halides must be investigated by including Hubbard U correction term to the calculations, so we added U from 0.5 to 3.0 eV which increases by successive 0.5 eV value and we determined the favorable magnetic ground states for each added U terms, we also repeated these calculations by adding U +SOC terms in our calculations. Relative ground state energy graphs can be found in S.M. Fig.S4.

According to our extended calculations, FM spin orientation is favorable just for $U=0.5$ eV both with and without SOC effect. For larger Hubbard energies zigzag (ZZ) orientation has minimum ground state energy comparing to others. We attained very close band gap value with experimentally obtained thin layered $\alpha\text{-RuCl}_3$ result⁴⁰ in our previous band structure calculations for RuCl_3 monolayer for Hubbard $U=1.5$ eV, thus we give in detail density of states for energetically favorable ZZ- RuX_3 (U +SOC and $U=1.5$ eV) monolayers in Fig. 3c. As can be seen in Fig 3c Hubbard U and SOC effects enhance the band gaps for RuX_3 monolayers and reaches 0.70 eV for RuBr_3 and 0.32 eV for RuI_3 . While t_{2g} orbitals of Ru atoms and p_x , p_y orbitals of I atoms determine the VBM level, all orbitals of Ru and Br atoms approximately give similar contribution at VBM. At conduction band minimums t_{2g} orbitals of Ru atoms are dominant. Calculated electronic band structures for all optimized RuX_3 monolayers, and also band trends can be found in S.M Fig. S5-S7.

IV. FROM BULK TO TWO-DIMENSIONAL MONOLAYER RuX_3 ; MONTE CARLO CALCULATIONS

A. Heisenberg-Kitaev Models

Recently, magnetic properties of certain materials exhibiting strong SOC have been modeled by using the Heisenberg-Kitaev (HK) model.⁴¹ For instance, magnetic

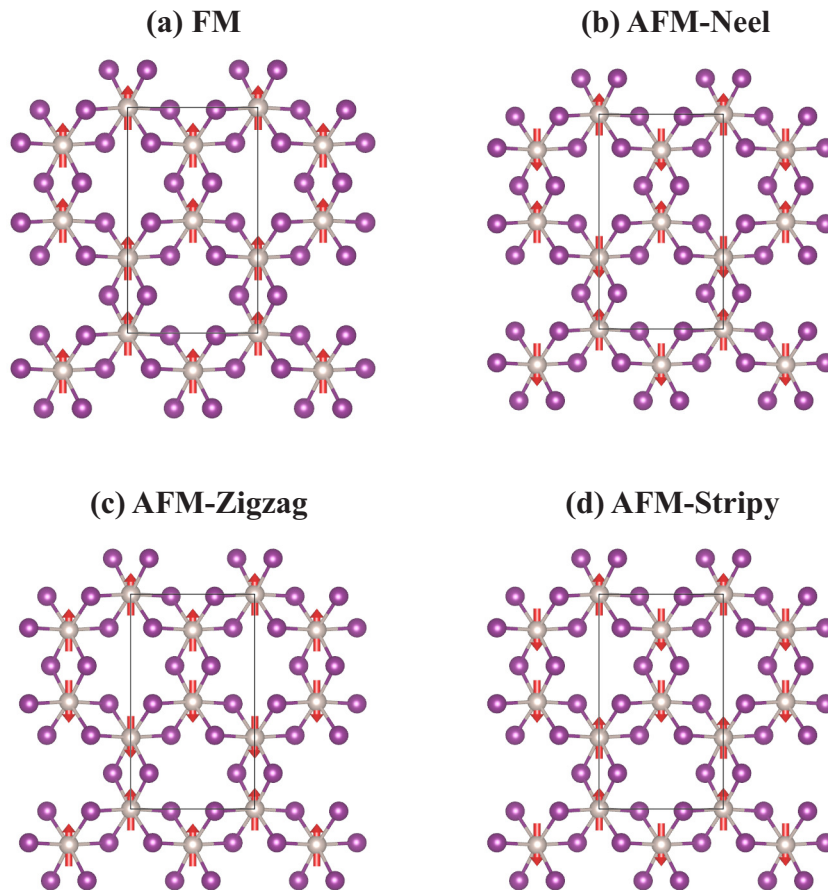


Figure 2. (Color online) Different spin configurations of the RuX_3 structures: (a) FM ordered, (b) AFM-Neel ordered, (c) AFM-Zigzag ordered and (d) AFM- stripy ordered.

behaviors of $\alpha - \text{RuCl}_3$ and Na_2IrO_3 have been studied by Janssen et al.⁴² They have demonstrated that the response of the system to an external field differs substantially for the different scenarios of stabilizing the zigzag state. The same group have also studied the honeycomb lattice HK model in an external magnetic field, and mapped out the classical phase diagram for different directions of the magnetic field.⁴³ In addition, magnetic behavior and phase diagrams of iridium oxides A_2IrO_3 have been investigated by Chaloupka and coworkers^{44,45} and by Singh et al.⁴⁶ The latter group have demonstrated that the magnetic properties of A_2IrO_3 can be modeled by using HK model including next-nearest neighbor interactions.

Apart from these works, there also exist several works dedicated to the investigation of magnetic properties of HK model in detail. For instance, the topological properties of the expanded classical HK model on a honeycomb lattice have been investigated by Yao and Dong.⁴⁷ The effect of the spatially anisotropic exchange couplings on the order-disorder characteristics of HK model has been clarified by Sela et al.⁴⁸ Classical HK model on a triangular lattice including the next-nearest neighbor inter-

actions and single ion anisotropy has been investigated by Yao.⁴⁹ Price and Perkins⁵⁰ elaborated the finite temperature phase diagram and order-disorder transitions of classical HK model on a hexagonal lattice. In a separate work,⁵¹ they have also studied the critical properties of the HK model on the honeycomb lattice at finite temperatures in which they have found that the model undergoes two phase transitions as a function of temperature. Finally, the relation between the classical HK model and quantum spin- S Kitaev model for large S has been discussed by Chandra et al.⁵²

Although Ising model is often utilized in determination of magnetic properties of real magnetic materials,²⁸ one may desire to take into account the apparent effect of MAE (see S.M Table S4) in the atomistic spin model calculations. Hence, for simplicity, we base our simulations on an anisotropic Heisenberg model. Although, classical Heisenberg model is a simple model in comparison to HK model, it provides physically more reasonable results in comparison to conventional Ising model which is only suitable for highly anisotropic magnetic systems.

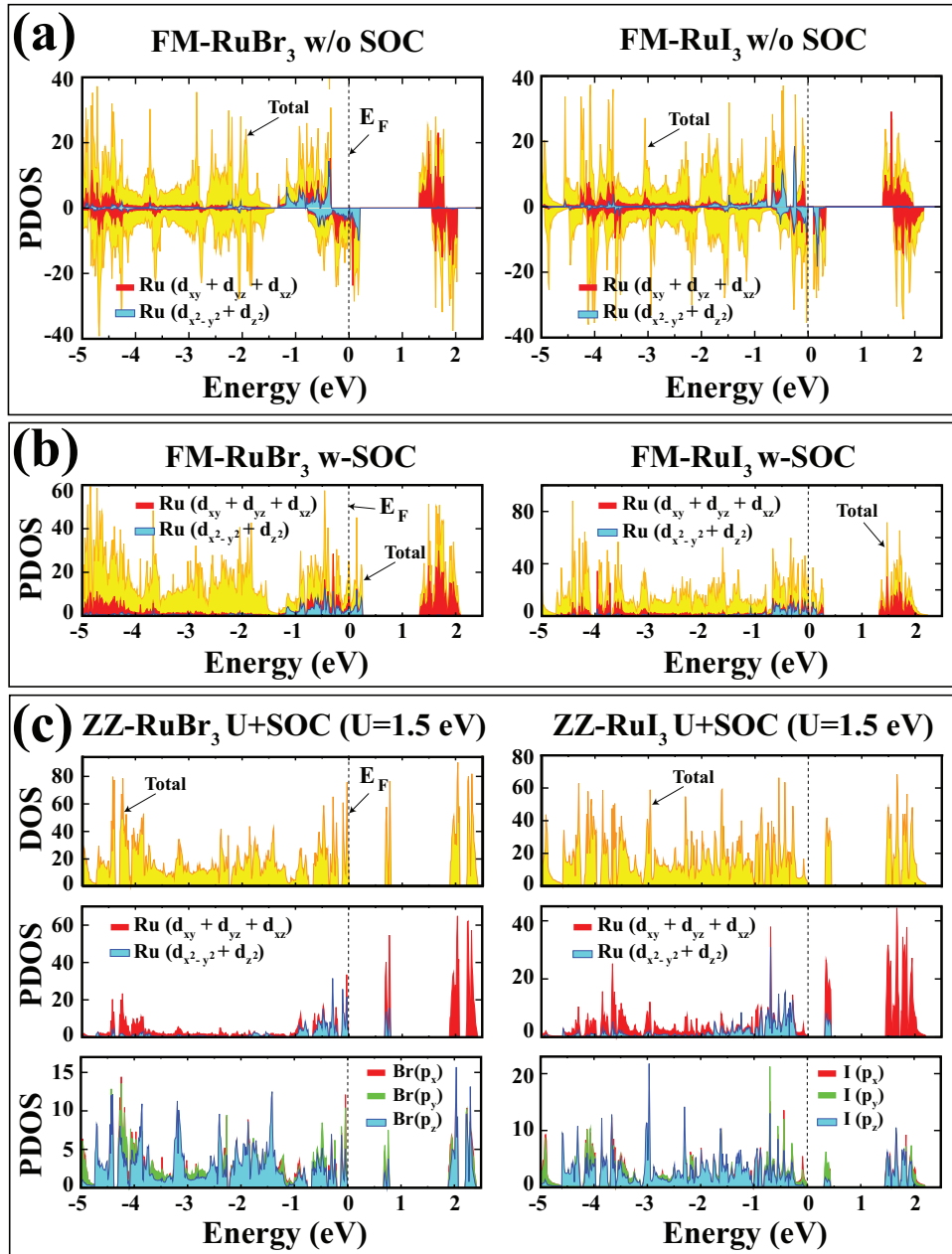


Figure 3. (Color online) Electronic PDOS (states/eV) of monolayer RuBr₃ and RuI₃ a) Total and d orbital contribution in DOS for FM-RuX₃ which calculated by PBE, b) total and d orbital contribution in DOS for FM-RuX₃ which calculated by PBE+SOC, c) Total density of states, partial orbital contribution of ruthenium and halogen atoms are given separately for ZZ-RuX₃ which is calculated with Hubbard U +SOC ($U=1.5$ eV) effect.

B. Monte Carlo Simulation Details

In order to clarify the magnetic properties of RuX₃ ($X = \text{Br}, \text{I}$), we proposed an atomistic spin model, and performed MC simulations based on the Metropolis algorithm⁵³ on a two dimensional honeycomb lattice with lateral dimensions $L_x = L_y = 100$ which contains $N = 10^4$ spins. We run our simulations based on the Hamiltonian defined by Eq.(1). The numerical values of system parameters have been provided in S.M Table

S3 and S4. According to Eq. (1), a Ru atom with a pseudo spin $|\mathbf{S}_i| = 1/2$ resides on each lattice site. We can briefly outline the simulation procedure based on Eq. (1) as follows: Starting from a high temperature spin configuration, we progressively cool down the system until the temperature reaches $T = 10^{-2}K$. We performed sequential spin flip update in our calculations with 10^5 MC steps per site where 10% of this value have been discarded for thermalisation. Periodic boundary conditions (PBC) were imposed in all directions. In order to reduce the

statistical errors, we performed 100 independent runs at each temperature. Error bars were calculated using the Jackknife method.⁵³ During the simulation, the following physical properties have been monitored:

- Time series of the spatial components of total magnetization

$$m_\alpha(t) = \frac{1}{N} \sum_{i=1}^N g\mu_B S_i^\alpha, \quad \alpha = x, y, z \quad (4)$$

where g is the Landé factor, and μ_B is the Bohr magneton. Using Eq. (4), we can obtain the thermal average of the magnitude of the total magnetization vector M_T , as well as its components M_α according to the following relations

$$\langle M_\alpha \rangle = \langle m_\alpha(t) \rangle, \quad \langle M_T \rangle = \left\langle \sqrt{\sum_{\alpha=x,y,z} m_\alpha^2(t)} \right\rangle. \quad (5)$$

- In order to locate the transition temperature, we have also calculated the thermal average of magnetic susceptibility χ and magnetic specific heat as follows

$$\chi = N(\langle M_T^2 \rangle - \langle M_T \rangle^2)/k_B T, \quad (6)$$

$$C = N(\langle \mathcal{H}^2 \rangle - \langle \mathcal{H} \rangle^2)/k_B T^2. \quad (7)$$

where k_B is the Boltzmann's constant. For the sake of completeness, we have also calculated the specific heat via

$$C = \frac{\partial \langle \mathcal{H} \rangle}{\partial T}. \quad (8)$$

C. Monte Carlo Simulation Results

In Fig. 4, we display the MC simulation results regarding the magnetic properties of simulated RuX_3 ($X = \text{Br, I}$) monolayer systems. In Fig. 4a, we plot the magnetization versus temperature for both structures. As seen in this figure, starting from high temperature configuration, as the temperature gradually decreases then the non zero magnetization components emerge. Since the out-of-plane anisotropy constants k_x and k_y equal to each other, main contribution to the total magnetization equally comes from x and y components whereas z component does not contribute to the magnetic behavior. Although the components exhibit apparent fluctuations in the considered temperature range, the magnitude $\langle M_T \rangle$ of total magnetization exhibits rather smooth behavior with error bars smaller than the data points. At very low temperatures $\langle M_T \rangle$ saturates to unity which means that RuX_3 ($X = \text{Br, I}$) system exhibits ferromagnetic behavior at the ground state. This is consistent with results of our DFT calculations where we predicted that the stable ground state of RuX_3 ($X = \text{Br, I}$)

is FM. Thermal variation of internal energy is shown in Fig. 4b. Absolute value of $\langle \mathcal{H} \rangle$ at low temperature region is larger than that of the high temperature region. This is due to the fact that with increasing temperature, thermal fluctuations are enhanced, and the system evolves towards the paramagnetic regime. The transition temperature of RuX_3 monolayers can be determined by examining the magnetic susceptibility and specific heat curves which are depicted in Figs.4c and 4d. As seen in these figures, both response functions exhibit a peculiar peak in the vicinity of the magnetic phase transition temperature. According to our simulation results, transition temperature values separating the ferromagnetic phase from paramagnetic phase are found to be $T_c = 2.11K$ and $T_c = 13.0K$ for RuI_3 and RuBr_3 , respectively. Relatively small T_c for the former structure is a direct consequence of weak J_i values of this structure (see S.M Table S3 and S4). T_c value obtained for RuI_3 monolayer is reasonably below the value reported by Huang and coworkers.²⁸ The reason is straightforward based on two reasons. First, in Ref.,²⁸ the authors considered only the nearest neighbor exchange interactions with $J_1 = 82$ meV which is fairly larger than our predicted value. Second, they omitted the effect of MAE (it seems that MAE is rather influential in RuX_3 , see Table S.M Table S4) in their calculations. On the other hand, T_c value obtained for RuBr_3 can be compared with $T_c = 14.21K$ for RuCl_3 reported in our recent work.²⁵ We note that recently it has also been reported for 2D ferromagnetic monolayers CrX_3 ($X=\text{Br, I}$) that Curie temperature of CrBr_3 is lower than that obtained for CrI_3 .²⁶ This is an opposite scenario in comparison to our reported values for RuX_3 where the Curie temperature of RuBr_3 is larger than that of RuI_3 . These results show that the presence of Ru instead of Cr in monolayer trihalides MX_3 ($X = \text{Br, I}$) may cause dramatic differences in critical behavior of these structures. Moreover, as we mentioned before, based on our rigorous DFT calculations, we believe that the magnetic behavior of such systems cannot be modeled using standard Ising model, since the MAE plays a significant role in the magnetic behavior of these materials. Therefore we suggest to use the anisotropic Heisenberg model in atomistic spin model calculations.

Apart from these observations, using the Hamiltonian parameters provided in S.M Table S3 and S4, we have also performed MC simulations for the bulk RuX_3 ($X = \text{Br, I}$). By assuming weak van der Waals bonding between adjacent magnetic interlayers,^{7,15,54} we followed the same simulation procedure defined for our monolayer systems. According to our simulation data, we found that the transition temperatures for RuI_3 and RuBr_3 in bulk form are given as $T_c = 0.11K$ and $T_c = 13.3K$, respectively. We note that although the Curie temperature of monolayer RuBr_3 is comparable to its bulk counterpart, the situation is different for RuI_3 where the critical temperature of the bulk system is lower than that of the monolayer system. This is primarily due to the fact that while the values of the exchange inter-

actions for monolayer and bulk cases are in the same order for RuBr_3 , the bulk exchange coupling parameters of RuI_3 predicted by our DFT calculations have been found to be fairly weaker than those calculated for the monolayer case (c.f. S.M Table S3). This means that a small amount of thermal fluctuation can be enough to destroy the magnetic order for the bulk RuI_3 system. Based on a recent experimental work,¹⁸ bulk to monolayer transition in CrI_3 have been reported with respective transition temperatures $T_c = 61\text{K}$ (bulk) and $T_c = 45\text{K}$ (monolayer). From this point of view, we have an opposite scenario where our RuI_3 system in bulk form exhibits lower critical temperature than that obtained for the monolayer limit. Hence, we can conclude that due to the presence of Ru instead of Cr in trihalides of the form MX_3 ($X = \text{Br}, \text{I}$), the bulk magnetic properties may also be significantly altered. This can be a direct consequence of different spin magnitudes of Ru and Cr, different exchange energies in the intralayer, as well as interlayer regions, etc.. In conclusion, one cannot establish a general trend for the critical behavior (i.e. variation of the critical temperature with the spatial dimension) of RuX_3 ($X = \text{Br}, \text{I}$) when the topology evolves from bulk to monolayer.

V. SUPPLEMENTARY MATERIAL

See supplementary material for the exchange interaction parameters such as J_1 , J_2 and J_3 , phonon band structures of bulk RuX_3 , electronic density of states of monolayer RuX_3 , relative energy differences for each configurations with respect to U and U+SOC parameters and compared band structures of monolayer RuX_3 in NM, FM, Neel, Stripy and Zigzag magnetic order using U+SOC methods.

VI. CONCLUSION

In conclusion, with the help of first principles calculations we theoretically showed that bulk RuBr_3 and RuI_3 could be stable in $\text{P3}_1\text{12}$ space group similar to $\alpha\text{-RuCl}_3$. According to cleavage energy calculations, monolayer forms of RuX_3 structures can be easily attained from their bulk phases. Also we tested dynamical and thermal stabilities of monolayers and found that they can be stable at room temperature and above. While ferromagnetic spin orientation is favorable state for PBE and PBE+SOC calculations, Hubbard U and U+SOC calculations show that AFM-zigzag cases have minimum ground state energies comparing to others except for $U=0.5$ eV. However, electronic band structures of all spin oriented configurations show similarities, U and SOC effects enhance the band gaps. While RuI_3 monolayer has band gaps values in the range of infrared region, band gap values of RuBr_3 monolayer can reach the near visible region according to spin orientation configuration and U

parameter. We have also performed detailed Monte Carlo simulations to clarify the magnetic properties of RuBr_3 and RuI_3 . Using the atomistic model parameters (i.e. exchange and magnetic anisotropy energies) obtained from PBE+SOC calculations, we have found that the Curie temperature of RuBr_3 dominates against that of RuI_3 both in bulk and monolayer forms. However, obtained critical temperature values are found to be far from the room temperature. Furthermore, some drastic changes may originate in the magnetic behavior of these systems when the form is changed from bulk to monolayer. According to the DFT calculations based on U+SOC, ground state configuration evolves from ferromagnetic to antiferromagnetic zigzag which causes prominent changes in the numerical values of simulation parameters (c.f. see S.M Tables S3, S6, S7). Besides, since the magnetic character of the first, second and third nearest neighbors turn into AFM type, RuX_3 system in bulk and monolayer phases exhibits Neel temperature instead of Curie temperature. More importantly, frustration effects take place in the system which completely affects the magnetic behavior. We should also note that, by comparing the magnetic anisotropy constants in the presence of U+SOC, we see that in the monolayer case, absolute values of the anisotropy constants attain lower values, in comparison to the case of PBE+SOC. In addition, in the monolayer case, anisotropy constants also lose their in plane isotropy (c.f. compare the numerical values of k_x and k_y between S.M. Tables S4 and S5). Overall, the entire magnetic behavior of RuX_3 ($X=\text{Br}, \text{I}$) may be highly sensitive to the consideration of Hubbard U parameter in DFT calculations. We believe that this study can play an important role, for the future attempt to obtain bulk and monolayer forms of RuBr_3 and RuI_3 .

ACKNOWLEDGMENTS

This work was supported by the Scientific and Technological Research Council of Turkey (TUBITAK) under the Research Project No. 117F133. Computing resources used in this work were provided by the TUBITAK ULAKBIM, High Performance and Grid Computing Center (Tr-Grid e-Infrastructure) and the National Center for High Performance Computing of Turkey (UHeM) under grant number 5004972017.

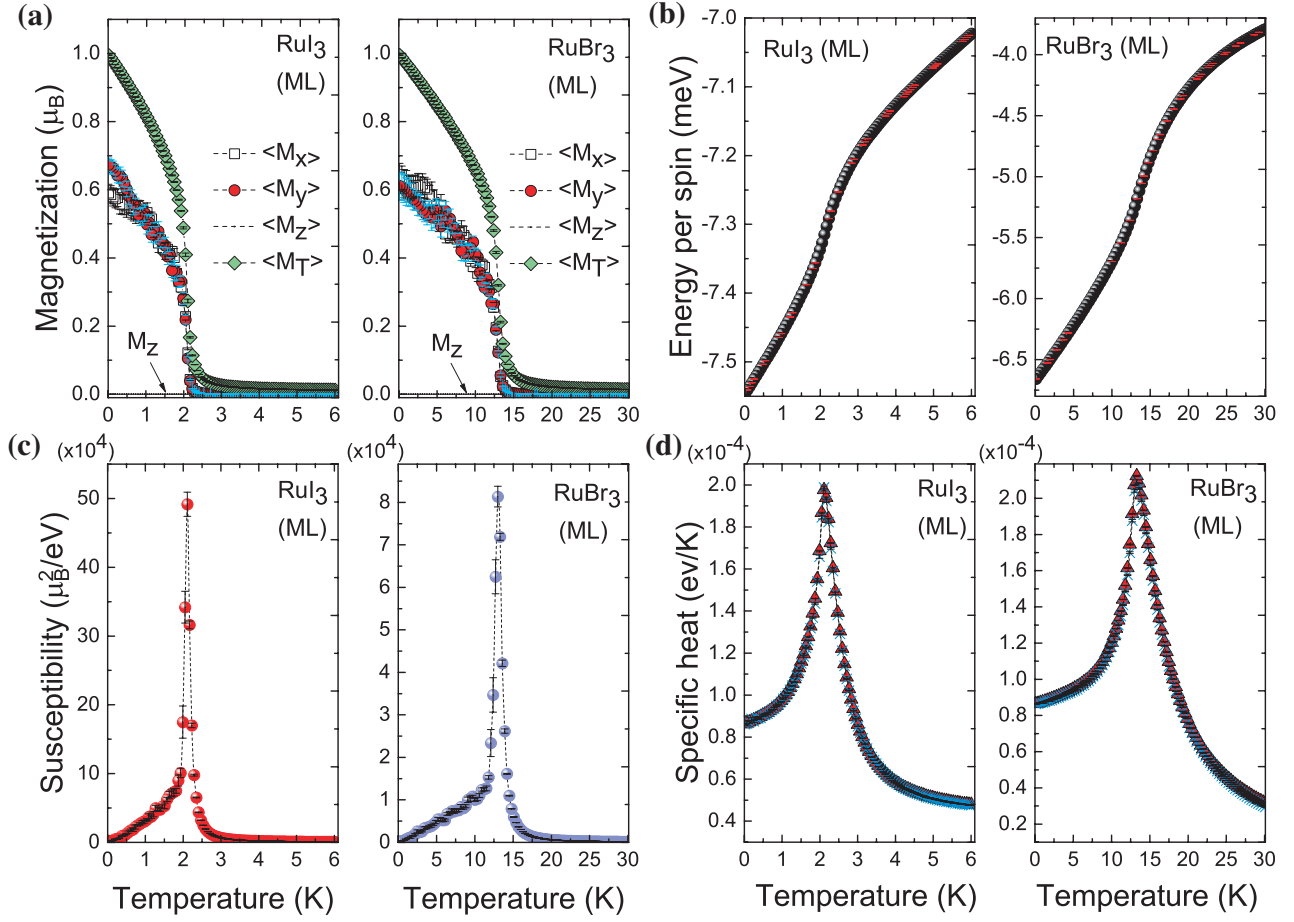


Figure 4. Temperature dependence of (a) average magnetization M_T and its components M_α , (b) average internal energy per spin, (c) magnetic susceptibility and (d) specific heat for RuI₃ and RuBr₃. In (d), different symbols denote the two distinct measurement methods for specific heat as discussed in Eq. (7) (Δ) and Eq. (8) (\times).

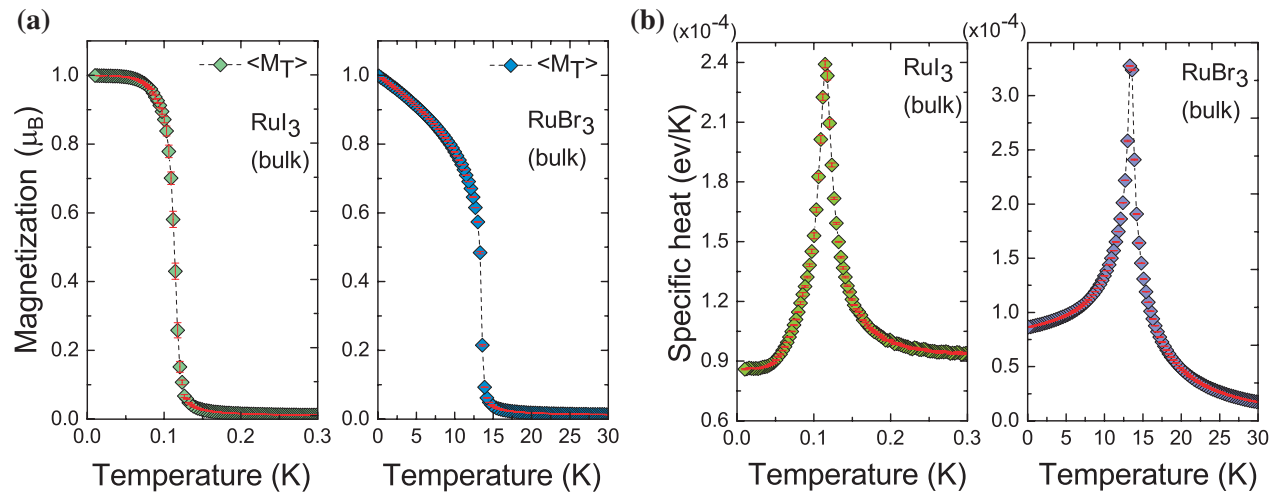


Figure 5. Temperature dependence of (a) average magnetization M_T and (b) specific heat for RuI₃ and RuBr₃ in bulk form. Specific heat curves have been obtained using Eq. (8).

* umit.akinci@deu.edu.tr

† ethem.akturk@adu.edu.tr

- ¹ Angelkort, J.; Senyshyn, A.; Schönleber, A.; Smaalen, S. v. Temperature-dependent neutron diffraction on TiI_3 . *Zeitschrift für Kristallographie Crystalline Materials* **2011**, *226*, 640–645
- ² Wang, H.; Eyert, V.; Schwingenschlögl, U. Electronic structure and magnetic ordering of the semiconducting chromium trihalides CrCl_3 , CrBr_3 , and CrI_3 . *Journal of Physics: Condensed Matter* **2011**, *23*, 116003
- ³ Wang, H.; Fan, F.; Zhu, S.; Wu, H. Doping enhanced ferromagnetism and induced half-metallicity in CrI_3 monolayer. *EPL (Europhysics Letters)* **2016**, *114*, 47001
- ⁴ Hillebrecht, H.; Ludwig, T.; Thiele, G. About Trihalides with TiI_3 Chain Structure: Proof of Pair Forming of Cations in $\beta\text{-RuCl}_3$ and RuBr_3 by Temperature Dependent Single Crystal X-ray Analyses. *Zeitschrift für anorganische und allgemeine Chemie* **2004**, *630*, 2199–2204
- ⁵ Zhou, Y.; Lu, H.; Zu, X.; Gao, F. Evidencing the existence of exciting half-metallicity in two-dimensional TiCl_3 and VCl_3 sheets. *Scientific reports* **2016**, *6*, 19407
- ⁶ Li, X.; Yang, J. First-principles design of spintronics materials. *National Science Review* **2016**, *3*, 365–381
- ⁷ Banerjee, A.; Bridges, C.; Yan, J.; Aczel, A.; Li, L.; Stone, M.; Granroth, G.; Lumsden, M.; Yiu, Y.; Knolle, J.; Bhattacharjee, S.. Proximate Kitaev quantum spin liquid behaviour in a honeycomb magnet. *Nature materials* **2016**, *15*, 733
- ⁸ Tsubokawa, I. On the magnetic properties of a CrBr_3 single crystal. *Journal of the Physical Society of Japan* **1960**, *15*, 1664–1668
- ⁹ Fletcher, J. M.; Gardner, W. E.; Hooper, E. W.; Hyde, K. R.; Moore, F. H.; Woodhead, J. L. Anhydrous ruthenium chlorides. *Nature* **1963**, *199*, 1089–1090
- ¹⁰ Baker, W.; Janus, A. Magnetic properties of Zirconium (III) and Hafnium (III) iodides. *Journal of Inorganic and Nuclear Chemistry* **1964**, *26*, 2087–2097
- ¹¹ Lin, J.; Miller, G. J. Dimensional diversity in transition metal trihalides. *Inorganic Chemistry* **1993**, *32*, 1476–1487
- ¹² Troyanov, S.; Snigireva, E.; Rybakov, V. X-ray-diffraction Study of Phase-transition in $\alpha\text{-TiCl}_3$. *ZHURNAL NE-ORGANICHESKOI KHIMII* **1991**, *36*, 1117–1123
- ¹³ Miró, P.; Audiffred, M.; Heine, T. An atlas of two-dimensional materials. *Chemical Society Reviews* **2014**, *43*, 6537–6554
- ¹⁴ Bengel, H.; Cantow, H.-J.; Magonov, S.; Hillebrecht, H.; Thiele, G.; Liang, W.; Whangbo, M.-H. Tip-force induced surface corrugation in layered transition metal trichlorides MCl_3 ($\text{M}=\text{Ru}, \text{Mo}, \text{Rh}, \text{Ir}$). *Surface science* **1995**, *343*, 95–103
- ¹⁵ Plumb, K.; Clancy, J.; Sandilands, L.; Shankar, V. V.; Hu, Y.; Burch, K.; Kee, H.-Y.; Kim, Y.-J. $\alpha\text{-RuCl}_3$: A spin-orbit assisted Mott insulator on a honeycomb lattice. *Physical Review B* **2014**, *90*, 041112
- ¹⁶ Weber, D.; Schoop, L. M.; Duppel, V.; Lippmann, J. M.; Nuss, J.; Lotsch, B. V. Magnetic properties of restacked 2D spin 1/2 honeycomb RuCl_3 nanosheets. *Nano letters* **2016**, *16*, 3578–3584
- ¹⁷ Dillon Jr, J.; Olson, C. Magnetization, Resonance, and Optical Properties of the Ferromagnet CrI_3 . *Journal of Applied Physics* **1965**, *36*, 1259–1260
- ¹⁸ Huang, B.; Clark, G.; Navarro-Moratalla, E.; Klein, D.; Cheng, R.; Seyler, K.; Zhong, D.; Schmidgall, E.; McGuire, M.; Cobden, D.; Yao, W. Layer-dependent ferromagnetism in a van der Waals crystal down to the monolayer limit. *Nature* **2017**, *546*, 270–273
- ¹⁹ McGuire, M.; Yan, J.; Lampen-Kelley, P.; May, A.; Cooper, V.; Lindsay, L.; Puzos, A.; Liang, L.; Santos, K.; Cakmak, E.; Calder, S. High-temperature magnetostructural transition in van der Waals-layered $\alpha\text{-MoCl}_3$. *Physical Review Materials* **2017**, *1*, 064001
- ²⁰ Zhang, W.-B.; Qu, Q.; Zhu, P.; Lam, C.-H. Robust intrinsic ferromagnetism and half semiconductivity in stable two-dimensional single-layer chromium trihalides. *Journal of Materials Chemistry C* **2015**, *3*, 12457–12468
- ²¹ He, J.; Ma, S.; Lyu, P.; Nichtigall, P. Unusual Dirac half-metallicity with intrinsic ferromagnetism in vanadium trihalide monolayers. *Journal of Materials Chemistry C* **2016**, *4*, 2518–2526
- ²² Kuzubov, A.; Kovaleva, E.; Popova, M.; Kholobina, A.; Mikhaleva, N.; Visotin, M.; Fedorov, A. DFT investigation of electronic structures and magnetic properties of halides family MeHal_3 ($\text{Me}=\text{Ti}, \text{Mo}, \text{Zr}, \text{Nb}, \text{Ru}$, $\text{Hal}=\text{Cl}, \text{Br}, \text{I}$) one dimensional structures. *Journal of Magnetism and Magnetic Materials* **2017**, *440*, 93–96
- ²³ McGuire, M. A. Crystal and Magnetic Structures in Layered, Transition Metal Dihalides and Trihalides. *Crystals* **2017**, *7*, 121
- ²⁴ Iyikanat, F.; Yagmurcukardes, M.; Senger, R.; Sahin, H. Tuning Electronic and Magnetic Properties of Monolayer $\alpha\text{-RuCl}_3$ by In-plane Strain. *Journal of Materials Chemistry C* **2018**, *6*, 2019–2025
- ²⁵ Sarikurt, S.; Kadioglu, Y.; Ersan, F.; Vatanserver, E.; Aktürk, O. Ü.; Yüksel, Y.; Akinci, Ü.; Aktürk, E. Electronic and magnetic properties of monolayer $\alpha\text{-RuCl}_3$: a first-principles and Monte Carlo study. *Physical Chemistry Chemical Physics* **2018**, *20*, 997–1004
- ²⁶ Liu, J.; Sun, Q.; Kawazoe, Y.; Jena, P. Exfoliating biocompatible ferromagnetic Cr-trihalide monolayers. *Physical Chemistry Chemical Physics* **2016**, *18*, 8777–8784
- ²⁷ McGuire, M. A.; Dixit, H.; Cooper, V. R.; Sales, B. C. Coupling of crystal structure and magnetism in the layered, ferromagnetic insulator CrI_3 . *Chemistry of Materials* **2015**, *27*, 612–620
- ²⁸ Huang, C.; Zhou, J.; Wu, H.; Deng, K.; Jena, P.; Kan, E. Quantum anomalous Hall effect in ferromagnetic transition metal halides. *Physical Review B* **2017**, *95*, 045113
- ²⁹ Kresse, G.; Furthmüller, J. Efficient iterative schemes for ab initio total-energy calculations using a plane-wave basis set. *Phys. Rev. B* **1996**, *54*(16), 11169
- ³⁰ Kresse, G.; Furthmüller, J. Efficiency of ab-initio total energy calculations for metals and semiconductors using a plane-wave basis set. *Comput. Mater. Sci.* **1996**, *6*(1), 15–50
- ³¹ Perdew, J. P.; Chevary, J. A.; Vosko, S. H.; Jackson, K. A.; Pederson, M. R.; Singh, D. J.; Fiolhais, C. Atoms, molecules, solids, and surfaces: Applications of the generalized gradient approximation for exchange and correlation. *Phys. Rev. B* **1992**, *46*, 6671
- ³² Perdew, J. P.; Burke, K.; Ernzerhof, M. Generalized gradient approximation made simple. *Phys. Rev. Lett.* **1996**, *77*, 3865

- ³³ Blöchl, P. E. Projector augmented-wave method. *Phys. Rev. B* **1994**, *50*, 17953
- ³⁴ Kresse, G.; Joubert, D. From ultrasoft pseudopotentials to the projector augmented-wave method. *Phys. Rev. B* **1999**, *59*, 1758
- ³⁵ Monkhorst, H. J.; Pack, J. D. Special points for Brillouin-zone integrations. *Phys. Rev. B* **1976**, *13*, 5188
- ³⁶ Togo, A.; Tanaka, I. First principles phonon calculations in materials science. *Scripta Mater.* **2015**, *108*, 1–5
- ³⁷ Sivadas, N.; Daniels, M. W.; Swendsen, R. H.; Oakamoto, S.; Xiao, D. Magnetic ground state of semiconducting transition-metal trichalcogenide monolayers. *Phys. Rev. B: Condens. Matter Mater. Phys.* **2015**, *91*, 235425
- ³⁸ Angelkort, J.; Schonleber, A.; van Smaalen, S. Low- and high-temperature crystal structures of TiI_3 . *Journal of Solid State Chemistry* **2009**, *182*, 525–531
- ³⁹ Tan, C.; Cao, X.; Wu, X.-J.; He, Q.; Yang, J.; Zhang, X.; Chen, J.; Zhao, W.; Han, S.; Nam, G.-H.; Sindoro, M.; Zhang, H. Recent Advances in Ultrathin Two-Dimensional Nanomaterials. *Chem. Rev.* **2017**, *117* (9), 6225–6331
- ⁴⁰ Ziatdinov, M.; Banerjee, A.; Maksov, A.; Berlijn, T.; Zhou, W.; Cao, H.; Yan, J.; Bridges, C.; Mandrus, D.; Nagler, S.; Baddorf, A. Atomic-scale observation of structural and electronic orders in the layered compound $\alpha\text{-RuCl}_3$. *Nature communications* **2016**, *7*, 13774
- ⁴¹ Kitaev, A. Anyons in an exactly solved model and beyond. *Ann. Phys.* **2006**, *321*, 2
- ⁴² Janssen, L.; Andrade, E. C.; Vojta, M. Magnetization processes of zigzag states on the honeycomb lattice: Identifying spin models for αRuCl_3 and Na_2IrO_3 . *Phys. Rev. B* **2017**, *96*, 064430
- ⁴³ Janssen, L.; Andrade, E. C.; Vojta, M. Honeycomb-lattice heisenberg-kitaev model in a magnetic field: Spin canting, metamagnetism, and vortex crystals. *Phys. Rev. Lett.* **2016**, *117*, 277202
- ⁴⁴ Chaloupka, J.; Jackeli, G.; Khaliullin, G. Kitaev-Heisenberg model on a honeycomb lattice: possible exotic phases in iridium oxides A_2IrO_3 . *Phys. Rev. Lett.* **2010**, *105*, 027204
- ⁴⁵ Chaloupka, J.; Jackeli, G.; Khaliullin, G. Zigzag magnetic order in the iridium oxide Na_2IrO_3 . *Phys. Rev. Lett.* **2013**, *110*, 097204
- ⁴⁶ Singh, Y.; Manni, S.; Reuther, J.; Berlijn, T.; Thomale, R.; Ku, W.; Trebst, S.; Gegenwart, P. Relevance of the Heisenberg-Kitaev model for the honeycomb lattice iridates A_2IrO_3 . *Phys. Rev. Lett.* **2012**, *108*, 127203
- ⁴⁷ Yao, X.; Dong, S. Topological triple-vortex lattice stabilized by mixed frustration in expanded honeycomb Kitaev-Heisenberg model. *Sci. Rep* **2016**, *6*, 26750
- ⁴⁸ Sela, E.; Jiang, H. C.; Gerlach, M. H.; Trebst, S. Order-by-disorder and spin-orbital liquids in a distorted Heisenberg-Kitaev model. *Phys. Rev. B* **2014**, *90*, 035113
- ⁴⁹ Yao, X. The expanded triangular Kitaev-Heisenberg model in the full parameter space. *Phys. Lett. A* **2014**, *378*, 2290
- ⁵⁰ Price, C.; Perkins, N. B. Finite-temperature phase diagram of the classical Kitaev-Heisenberg model. *Phys. Rev. B* **2013**, *88*, 024410
- ⁵¹ Price, C.; Perkins, N. B. Critical properties of the Kitaev-Heisenberg model. *Phys. Rev. Lett.* **2012**, *109*, 187201
- ⁵² Chandra, S.; Ramola, K.; Dhar, D. Classical Heisenberg spins on a hexagonal lattice with Kitaev couplings. *Physical Review E* **2010**, *82*, 031113
- ⁵³ Newman, M. E. J.; Barkema, G. T. *Monte Carlo Methods in Statistical Physics*
- ⁵⁴ Sears, J. A.; Songvilay, M.; Plumb, K. W.; Clancy, J. P.; Qiu, Y.; Zhao, Y.; Parshall, D.; Kim, Y.-J. Magnetic order in αRuCl_3 : A honeycomb-lattice quantum magnet with strong spin-orbit coupling. *Phys. Rev. B* **2015**, *91*, 144420

**VII. SUPPLEMENTARY
MATERIAL: EXPLORING THE ELECTRONIC
AND MAGNETIC PROPERTIES OF NEW
METAL HALIDES FROM BULK TO
TWO-DIMENSIONAL MONOLAYER: RuX_3
($\text{X}=\text{BR}, \text{I}$)**

A. Bulk RuX_3

Figure 6 illustrates the phonon band structure of bulk RuX_3 structures with comparable density of states and thermodynamic variables of their bulk and monolayer phases. Phonon dispersions show that all phonon modes have positive value in the whole Brillouin zone, which imply the dynamical stability at $T \sim 0\text{K}$. As can be seen from phonon DOS, there are only Br atoms vibrations in the range of 5-6 THz for RuBr_3 and I atoms vibrations in the range of 3-4.5 THz for RuI_3 bulk structures. Probably these dominant peaks could be seen in Raman spectrums. Thermodynamic variables are extracted from PHONOPY after the phonon calculations and given as a function of temperature. As can be seen, free energies of bulk and monolayer of RuX_3 structures go to negative values after about 200K, and also C_v , heat capacities become fixed for $T > 200\text{K}$ and tend to the Dulong-Petit limit.

We determine the favorable magnetic ground state of RuX_3 ($\text{X}=\text{Br}, \text{I}$) bulk structures with considering the Hubbard $U+\text{SOC}$ ($U=1.5\text{ eV}$) effect. As in the case for RuX_3 monolayer, we reveal that Zigzag spin orientation is energetically stable for bulk structures. We also performed electronic band structure calculation for RuX_3 ($\text{X}=\text{Br}, \text{I}$) bulk structures with Hubbard $U+\text{SOC}$ ($U=1.5\text{ eV}$) effect (Figure 7). We find out the energy band gaps as 0.62 eV and 0.22 eV for RuBr_3 and RuI_3 , respectively.

B. Spin orientation and exchange interaction energy

Since free Ruthenium and each halogen atoms has magnetization ($2\mu_B$ for Ru, and $1\mu_B$ for halogens), spin orientation in the structure which includes these atoms, will have an important role to determine the ground state energy of the system. Hence, we optimized all structures for various Hubbard U parameters with and without SOC parameters for all considered spin orientations and obtained their ground state energies. Figure 9 illustrates the relative ground state energies with respect to Hubbard parameters. Generally for small U parameter ($U=0.5\text{ eV}$) ferromagnetic spin orientation is favorable state, but with increasing U value zigzag orientation becomes energetically favorable. We also calculated exchange interaction energy for PBE, PBE+SOC, U and $U+\text{SOC}$ calculations as seen in Table III, VI, VII. These extended calculations show that exchange interaction energy increases with increasing of U energy.

C. Electronic properties of RuX_3 monolayers

Figure 10, 12, 11 show the band gap trend and band structures of all considered spin oriented RuX_3 monolayers for various U and $U+\text{SOC}$ parameters. As can be seen from the band structures, increasing of U value enhances the band gaps. For FM spin oriented structures Hubbard U Coulomb interaction effective after $U=2\text{ eV}$ for RuBr_3 , while this U value is 3 eV for RuI_3 monolayer. FM band structures are plotted for only spin-up channels due to spin-down channels have huge band gaps values, which are very out of the scales that plotted.

Table I. Calculated relative energy values in meV/atom (E_{rel}) which are obtained from the PBE, PBE+SOC and U+SOC (U=1.5 eV) calculations for bulk RuX_3 (X=Br,I). Zero of energy refers the ground state energy.

		FM	Neel	Stripy	Zigzag
RuBr ₃	E_{rel}^{PBE}	0	13.63	5.58	6.69
	$E_{rel}^{PBE+SOC}$	0	9.46	4.86	4.22
	E_{rel}^{U+SOC}	20.82	2.00	1.89	0
RuI ₃	E_{rel}^{PBE}	0	1.99	1.86	1.76
	$E_{rel}^{PBE+SOC}$	0	0.02	0.02	0.02
	E_{rel}^{U+SOC}	9.5	0.18	8.69	0

Table II. Calculated relative energy values in meV/atom (E_{rel}) which are obtained from the PBE and PBE+SOC calculations for monolayer RuX_3 (X=Br,I). Zero of energy refers the ground state energy.

		FM	NM	Neel	Stripy	Zigzag
RuBr ₃	E_{rel}^{PBE}	0	22.67	21.58	5.38	7.52
	$E_{rel}^{PBE+SOC}$	0	14.68	13.07	4.19	4.80
RuI ₃	E_{rel}^{PBE}	0	10.08	10.07	7.45	9.48
	$E_{rel}^{PBE+SOC}$	0	0.66	0.66	0.65	0.65

Table III. Calculated exchange interaction parameters J_1 , J_2 , J_3 (meV) for bulk and monolayer RuX_3 (X=Br,I) from the PBE and PBE+SOC calculations.

		J_1	J_2	J_3
RuBr ₃ (Bulk)	PBE	6.26	-0.34	2.82
	PBE+SOC	5.05	-0.093	1.25
	U+SOC (U=1.5 eV)	-8.46	-5.23	-4.08
RuBr ₃ (ML)	PBE	9.72	-2.17	4.66
	PBE+SOC	6.23	-1.02	2.48
RuI ₃ (Bulk)	PBE	1.11	0.44	0.21
	PBE+SOC	11.1×10^{-3}	4.02×10^{-3}	1.64×10^{-3}
	U+SOC (U=1.5 eV)	-0.31	-0.25	-5.9
RuI ₃ (ML)	PBE	4.02	1.72	2.69
	PBE+SOC	0.33	0.16	0.11

Table IV. Magneto-crystalline anisotropy energies and anisotropy constants for FM configuration of bulk and monolayer RuX_3 (X=Br,I) using PBE+SOC method.

	out-of-plane $E[100] - E[001]$	in-plane $E[100] - E[010]$	k_x (eV)	k_y (eV)
RuBr ₃ (Bulk)	-7.26 meV	-1.5 meV	-0.0073	-0.0088
RuBr ₃ (ML)	-16.65 meV	-16 μ eV	-0.017	-0.017
RuI ₃ (Bulk)	-17.5 meV	1.45 meV	-0.0175	-0.019
RuI ₃ (ML)	-29.04 meV	58 μ eV	-0.029	-0.029

Table V. Magneto-crystalline anisotropy energies and anisotropy constants for Zigzag configuration of bulk and monolayer RuX₃ (X=Br,I) using U+SOC method (U=1.5 eV).

	out-of-plane $E[100] - E[001]$	in-plane $E[100] - E[010]$	k_x (eV)	k_y (eV)
RuBr ₃ (Bulk)	-5.26 meV	-0.36 meV	-0.0053	-0.0049
RuBr ₃ (ML)	-5.26 meV	-0.35 meV	-0.0052	-0.0049
RuI ₃ (Bulk)	-13.19 meV	1.21 meV	-0.0144	-0.0132
RuI ₃ (ML)	-12.88 meV	-4.27 meV	-0.0129	-0.0086

Table VI. Calculated exchange interaction parameters J_1, J_2, J_3 (meV) for monolayer RuBr₃ using the U and U+SOC methods.

	w/o SOC			w SOC		
U	J_1	J_2	J_3	J_1	J_2	J_3
0.5	3.18	-0.19	1.64	4.46	-1.11	1.62
1.0	3.79	-1.25	0.07	-2.82	-2.77	-2.63
1.5	18.15	4.63	-23.05	-11.04	-6.40	-4.78
2.0	17.34	7.34	-32.79	-19.56	-10.41	-7.39
2.5	17.03	29.76	-15.73	-27.20	-13.96	-9.57
3.0	17.42	39.63	-16.29	-6.40	-41.78	-57.82

Table VII. Calculated exchange interaction parameters J_1, J_2, J_3 (meV) for monolayer RuI₃ using the U and U+SOC methods.

	w/o SOC			w SOC		
U	J_1	J_2	J_3	J_1	J_2	J_3
0.5	6.13	1.42	1.10	1.15	-0.15	-0.58
1.0	8.08	-0.63	-1.28	-1.78	-1.71	-2.15
1.5	13.09	-3.02	-7.24	-8.14	-4.71	-3.92
2.0	22.94	-4.48	-17.41	0.77	-0.12	-0.72
2.5	4.379	-21.39	1.52	0.74	-0.038	-0.57
3.0	3.80	-29.88	2.31	0.66	-0.004	-0.42

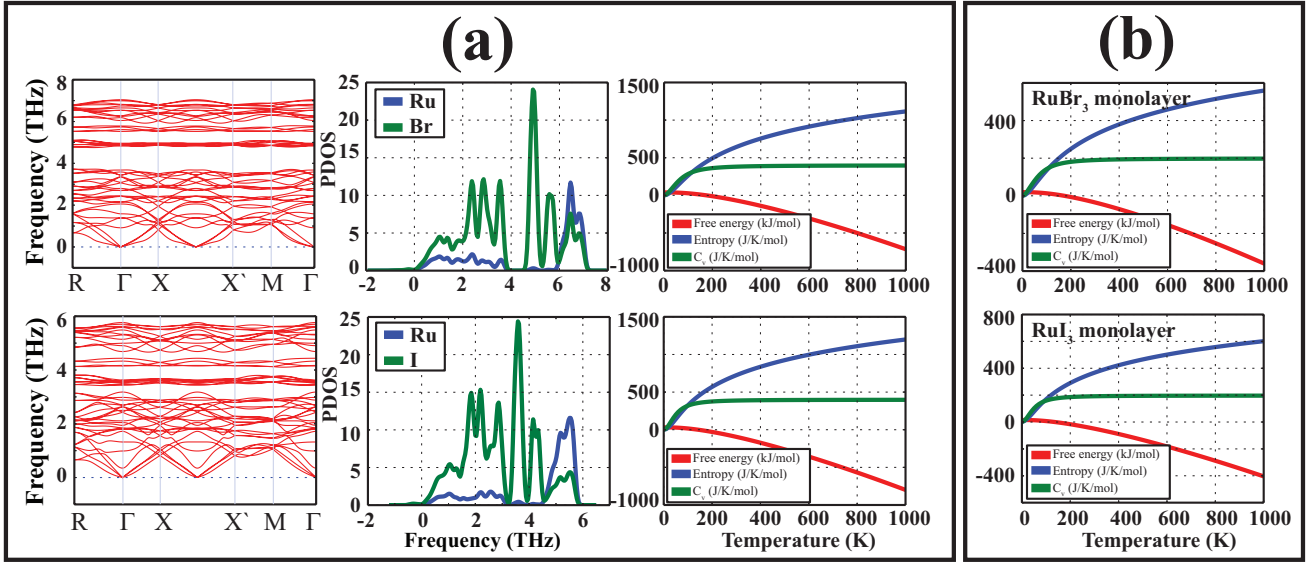


Figure 6. (Color online) a) Phonon band structure, phonon partial density of states and thermodynamic properties as a function of temperature of bulk ($P3_112$ space group) RuBr_3 and RuI_3 structures, b) thermodynamic properties as a function of temperature of monolayer RuBr_3 and RuI_3 structures.

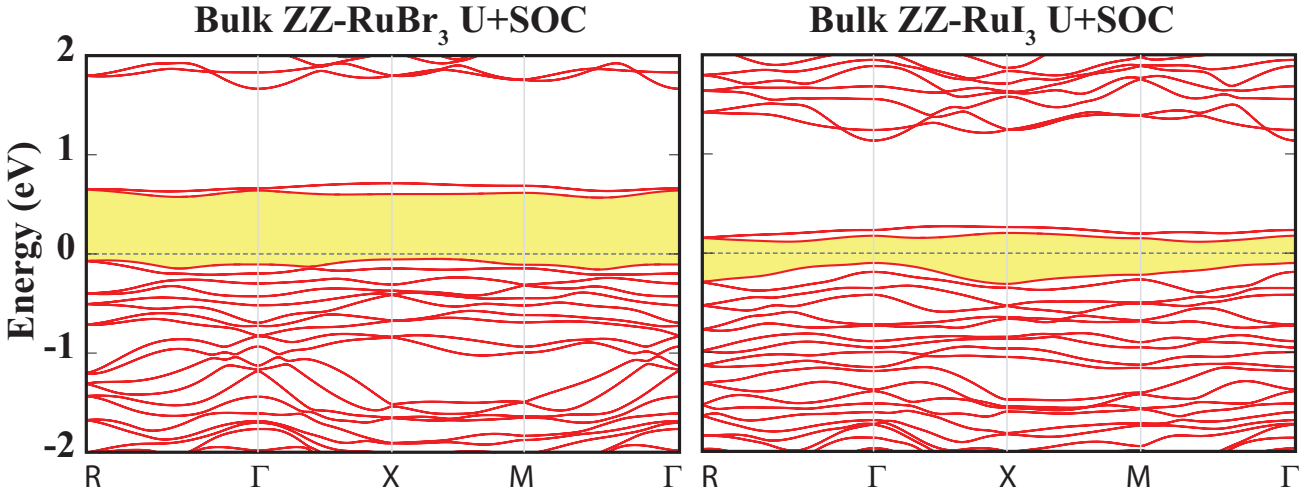


Figure 7. (Color online) Electronic band structure of bulk RuX_3 ($X=\text{Br}, \text{I}$) in Zigzag magnetic order using $U+\text{SOC}$ methods ($U=1.5$ eV). Fermi energy is set to zero energy and band gaps are colored.

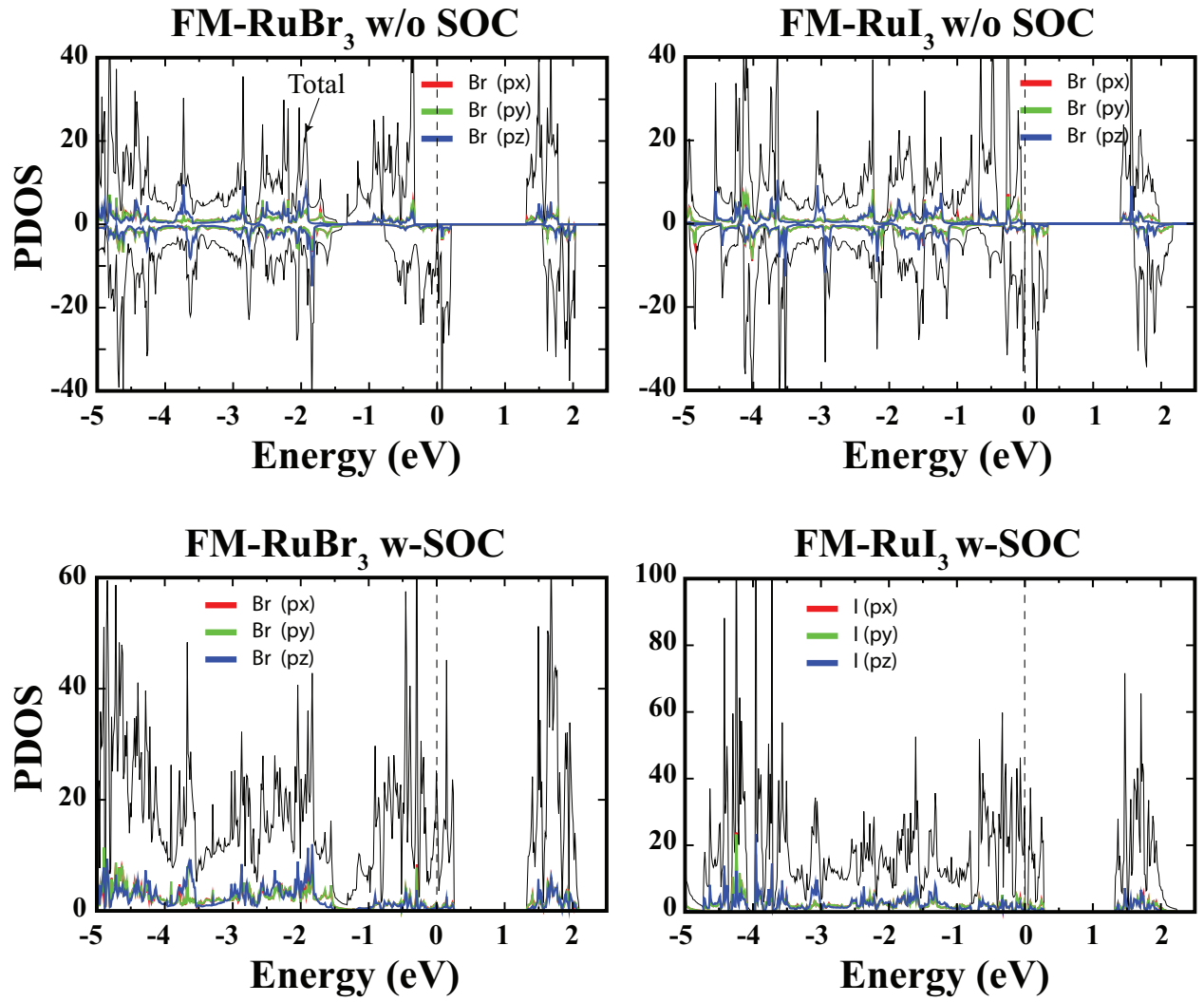


Figure 8. (Color online) Electronic partial density of states of RuBr_3 and RuI_3 monolayers, which are obtained from the PBE and PBE+SOC calculations.

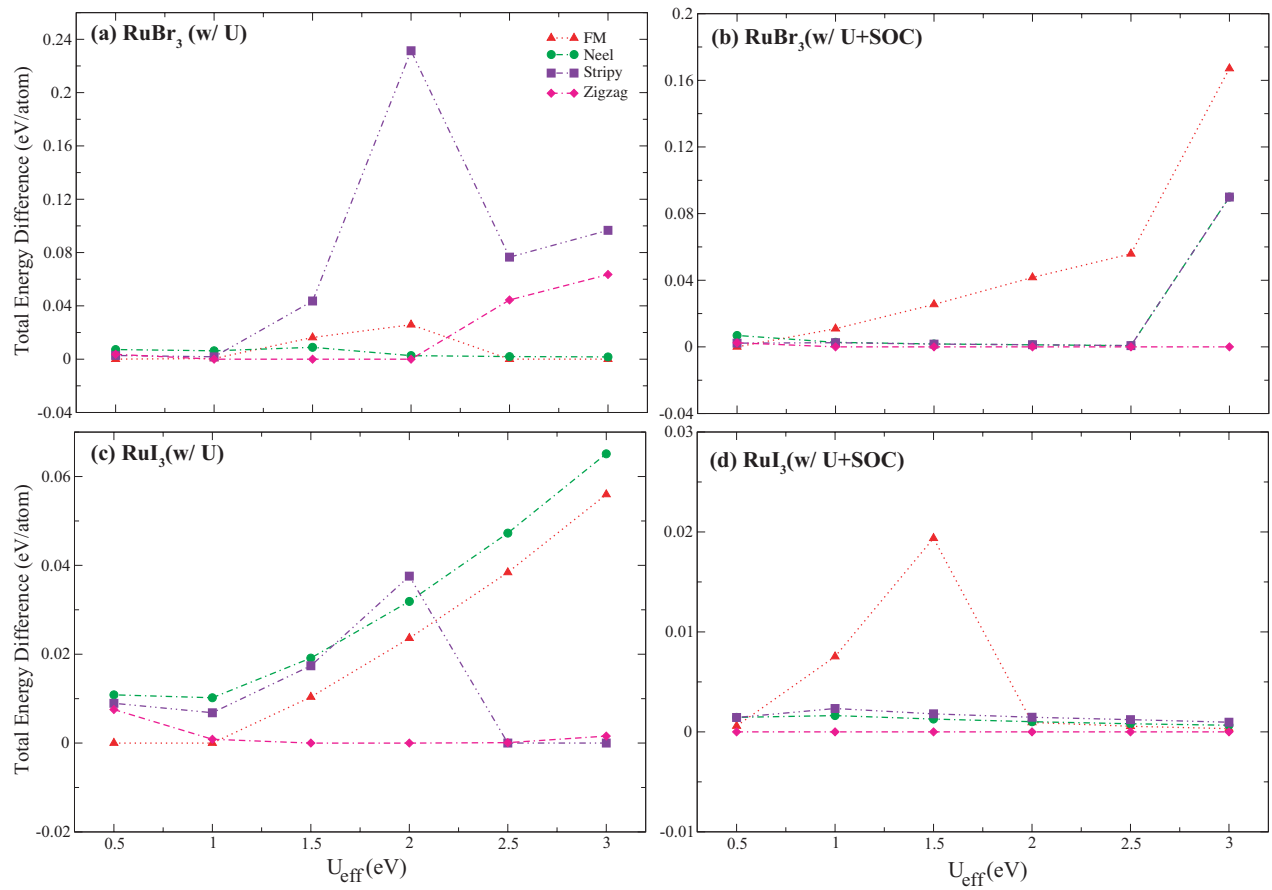


Figure 9. (Color online) Relative energy difference for each configuration with respect to U_{eff} using the U and U+SOC methods. (a)-(b) RuBr₃ monolayer (c)-(d) RuI₃ monolayer. Zero of energy refers the ground state energy.

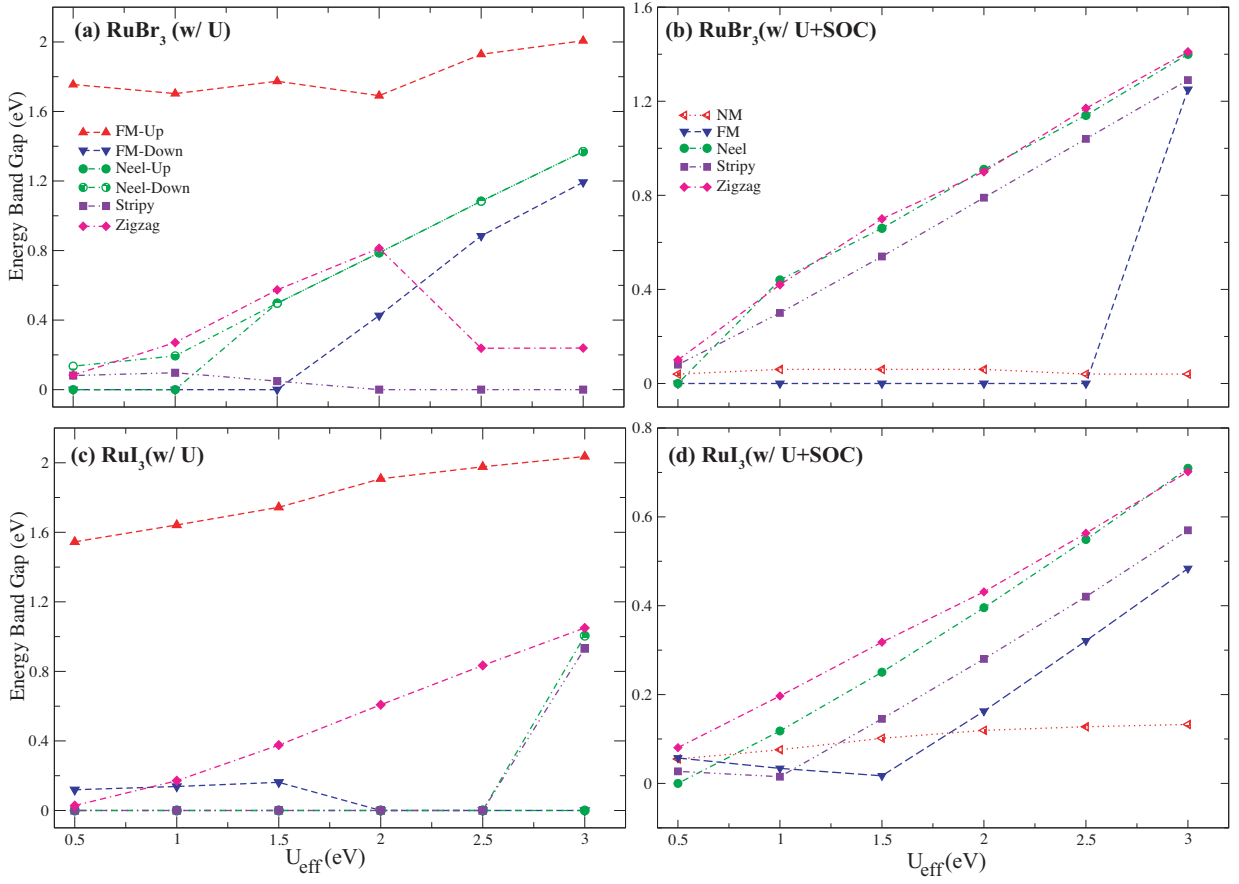


Figure 10. (Color online) Calculated energy band gap values of all magnetic configurations as a function of U_{eff} using the U and U+SOC methods. U results are depicted in (a) and (c) for RuBr₃ and RuI₃, respectively. U+SOC results are given in (b) and (d) for RuBr₃ and RuI₃, respectively.

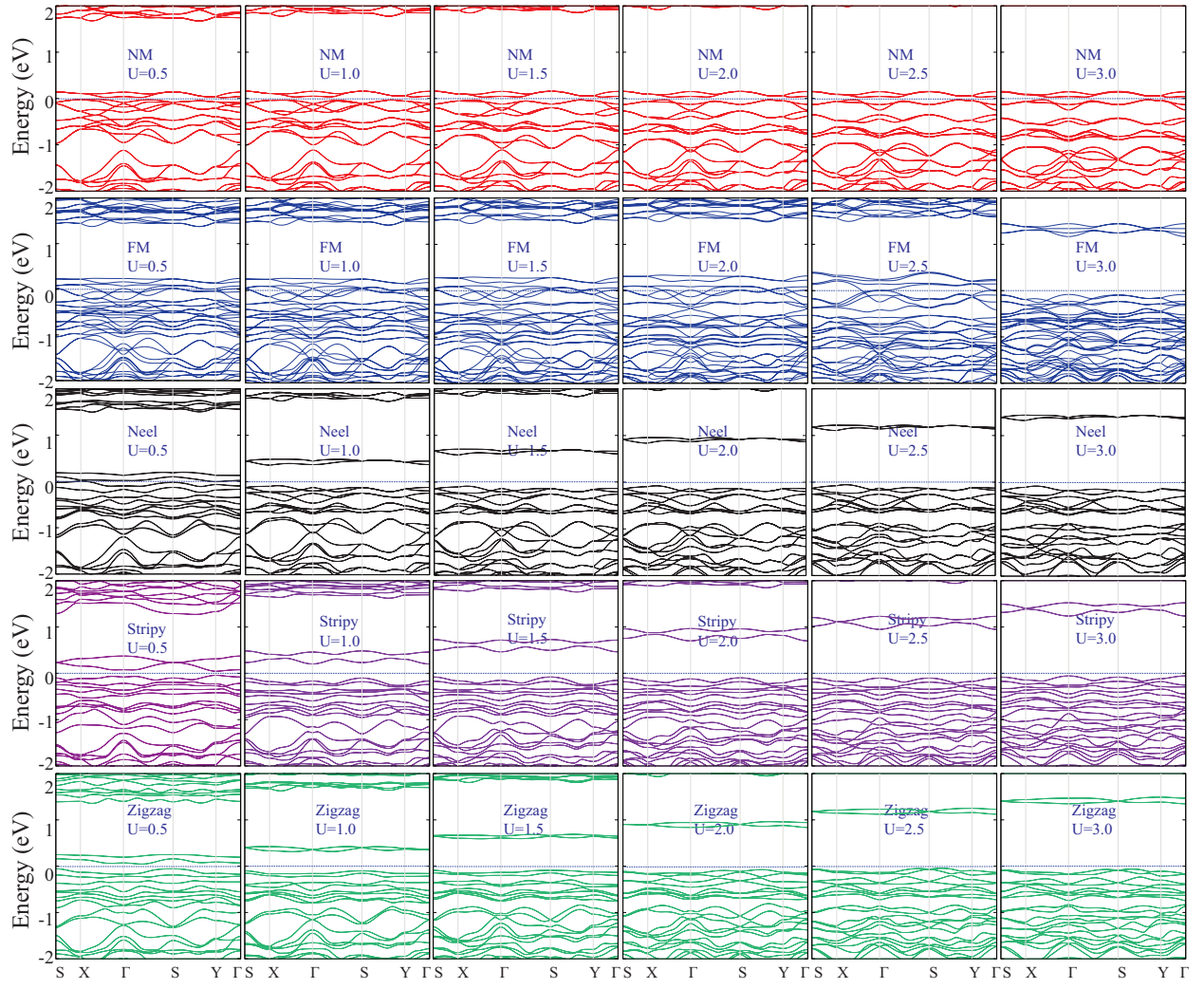


Figure 11. (Color online) The effect of on-site Coulomb interaction on the electronic structure of monolayer RuBr_3 in NM, FM (only for spin-up channels), Neel, Stripy and Zigzag magnetic order using U+SOC methods.

